

Microscopic approach to the kinetics of pattern formation of charged molecules on surfacesV. N. Kuzovkov,^{1,*} G. Zvejnieks,¹ E. A. Kotomin,¹ and M. Olvera de la Cruz^{2,†}¹*Institute of Solid State Physics, University of Latvia, 8 Kengaraga Street, LV-1063 Riga, Latvia*²*Department of Materials Science and Engineering, Northwestern University, Evanston, Illinois 60208, USA*

(Received 4 May 2010; published 9 August 2010)

A microscopic formalism based on computing many-particle densities is applied to the analysis of the diffusion-controlled kinetics of pattern formation in oppositely charged molecules on surfaces or adsorbed at interfaces with competing long-range Coulomb and short-range Lennard-Jones interactions. Particular attention is paid to the proper molecular treatment of energetic interactions driving pattern formation in inhomogeneous systems. The reverse Monte Carlo method is used to visualize the spatial molecular distribution based on the calculated radial distribution functions (joint correlation functions). We show the formation of charge domains for certain combinations of temperature and dynamical interaction parameters. The charge segregation evolves into quasicrystalline clusters of charges, due to the competing long- and short-range interactions. The clusters initially co-exist with a gas phase of charges that eventually add to the clusters, generating "fingers" or line of charges of the same sign, very different than the nanopatterns expected by molecular dynamics in systems with competing interactions in two dimensions, such as strain or dipolar versus van der Waals interactions.

DOI: [10.1103/PhysRevE.82.021602](https://doi.org/10.1103/PhysRevE.82.021602)

PACS number(s): 68.43.-h, 81.16.Rf, 81.65.Cf, 89.75.Kd

I. INTRODUCTION

Patterning of surfaces is of paramount importance in biotechnology [1,2]. In particular, charged patterns generated by the adsorption of cationic and anionic molecules on surfaces and on membranes made of cationic and anionic components is of great importance in electrochemistry and biophysics. The surface structural properties of these charged systems are of interest because surfaces and interfaces are highly catalytic [3–7]. Furthermore, charged components on surfaces generate functionality [8] including helicity [9], as well as ionic faceting [10]. Surfaces with ionic components have the unique advantage to be readily modified without mechanical intervention by simply changing the ionic conditions and/or pH values. For example, in flat surfaces dense systems of cationic and anionic molecules form a large variety of charged patterns [11,12], which are modified by changing the ionic strength. Moreover, when a charged molecule approaches an ionic interface, the surface ionic components redistribute themselves accordingly so as to induce a strong polarizability on the approaching charged molecule, which in turn breaks the symmetry of the molecule as well as the surface ionic pattern [13].

Periodic and spatially organized surfaces are a result of competing interactions, and they occur in different systems that include magnetic systems [14,15] or asymmetric molecules with dipolar interactions [16], in block copolymers [17] and in system undergoing chemical reactions [1,18]. In particular, patterns of ionic components on surfaces can have a much richer phase behavior, given that the long-range interaction can propagate through the media in the third dimension, in addition to their tuneability using external conditions, including the presence of an electric field. As such,

pattern formation and phase separation in surface and interfacial systems of oppositely charged molecules are of fundamental importance not only in biological membranes but also to generate functional devices. Indeed, patterns of positively and negatively charges on surface have been generated and analyzed for a large variety of applications [19]. In dilute and semidilute ionic conditions as well as in the presence of van der Waals or other short-range interactions existing among the adsorbed ionic components, a large variety of ionic patterns on surfaces, which co-exists with dilute ionic solutions on surfaces, can be induced [20]. Ionic pattern of mixed nanoparticles also produce patterns characterized as Liesegang Rings [12]. Charged patterns are also observed using AC external fields [21].

Currently, most theoretical works on pattern formation and phase separation in condensed matter focus on techniques performed at the mesoscopic level where particle distributions are defined by the concentration fields [18,22]. Along with simple analytical methods, molecular dynamics (MD) simulations are also used, for instance, for the phase separation on a two-dimensional (2D) interface with oppositely charged adsorbed molecules [20]. In fact, this approach is actually predicated on the assumption that the equilibrium structure of such monolayer surface results from the classical Newtonian dynamics.

However, the issues of irreversibility in dynamical systems as well as the plausibility of even reaching the equilibrium remain open problems in the field of statistical physics [23–25]. Furthermore, there exists arguments that claim the observations of equilibrium results are entirely due to the limited accuracy in the numerical integration of the underlying dynamical equations. Above all, effects such as adsorbate-surface interaction have not been taken into account by conventional methods. We believe the efficient alternative approach is treating the molecules on the surface/interface as a random (Brownian) walk. In this case, the molecules are effectively characterized by their diffusion

*kuzovkov@latnet.lv

†m-olvera@northwestern.edu

coefficients instead of masses. As is well known, diffusion is an irreversible process, and as such, we suggest to use the diffusion dynamics in this study on how the system reaches the equilibrium.

We note that the density of the system considered in Ref. [20] is intermediate between a gas phase and condensed structure, so that these two phases can indeed co-exist. However, in systems with phase separation, the Ostwald ripening mechanism is known when small aggregates or molecules are absorbed by larger aggregates. This is a very slow process, and it is of great interest to study its kinetics toward equilibrium as well as its dependence on the microscopic parameters of the system.

Analytical treatment of the kinetics of the diffusion-controlled processes can often be accompanied by computer modeling based on the kinetic Monte Carlo (kMC) method. In fact, both MD and kMC have common disadvantages: in a mixture of charged molecules with underlying long-range potentials, the size of a modeled system is relatively small (see, for example, figures in [20]), thus, the statistics of the results is limited and transition to the thermodynamic limit thus hardly possible. As a rule, the results of modeling are illustrated by snapshots of several configurations whose selection is subjective. Our alternative approach is to get the kinetics of the transition toward equilibrium in the thermodynamical limit, using the same methods and accuracy that are commonly employed in the statistical physics of dense gases and liquids [23].

Obviously, there exists a wide gap between the mesoscopic language commonly used in the studies of pattern formation, as well as phase separation processes, and the microscopic (atomistic) language used in the statistics of equilibrium systems. Again, the latter approach is not widely used in the study of process kinetics. So far, there have been only a few pioneering attempts to predict the pattern size as well as short- and intermediate-range order in the reactant distribution using the microscopic level, e.g., using the formalism of the many-point particle densities [26,27]. These are very close to the radial distribution functions used in statistical physics, the knowledge of which permits one to calculate such observables as the structure factors.

In this work, we propose to combine the formalism of the many-point particle densities with the framework of reverse MC (RMC) [28–30] to study the kinetics of pattern formation on charged surface systems. Based on the calculated radial distribution functions, the reverse MC method permits us to obtain spatial configurations of the molecules that best fit (in terms of χ^2 distribution) these computed radial functions. Since the reverse problem is not uniquely defined, the obtained configurations should be considered as typical snapshots, similarly to those obtained in direct MD or kMC simulations. We discuss the patterns formed and compare to those obtained by molecular dynamics and Monte Carlo simulations in related systems, including the chains observed in simulations of the restricted primitive model (RPM), which does not have short range attractions among components, of cationic and anionic spherical ions [31,32]

II. METHODS

A. Many-point densities

1. Definitions

In what follows, we employ the formalism of the *many-point densities* for a number of particles as discussed in detail in [26,27]. Given two types of particles in the system, the many-point densities are functions of their respective coordinates, A and B : $\rho_{m,m'} \equiv \rho_{m,m'}(\{\mathbf{r}\}_m; \{\mathbf{r}'\}_{m'})$, where $\{\mathbf{r}\}_m = \mathbf{r}_1, \dots, \mathbf{r}_m$ and $\{\mathbf{r}'\}_{m'} = \mathbf{r}'_1, \dots, \mathbf{r}'_{m'}$. The quantity $\rho_{m,m'} d\mathbf{r}_1 \dots d\mathbf{r}_m d\mathbf{r}'_1, \dots, \mathbf{r}'_{m'}$ yields the *mean number of configurations* with m particles A in the volumes $d\mathbf{r}_i$ at \mathbf{r}_i ($i=1, \dots, m$) and m' particles B in the volumes $d\mathbf{r}'_j$ at \mathbf{r}'_j ($j=1, \dots, m'$).

In general, this formalism is not suitable for periodic systems with long-range order but works well in cases with an intermediate order such as dense gases and liquids (amorphous solids). This approach has so far been successfully applied in the analysis of pattern formation and critical phenomena, including *microscopic self-organization* [33]. Due to the translational invariance for the first two many-particle densities, $\rho_{1,0}$ and $\rho_{0,1}$ are coordinate-independent and coincide with the average A - and B -type particle densities, respectively, $\rho_{1,0} = n_A$ and $\rho_{0,1} = n_B$.

Since the system is also isotropic, the two-point densities depend only on the relative coordinates. Therefore, we now define three kinds of joint correlation functions based on the two-point densities [26,27]:

$$\rho_{2,0} = n_A^2 X_A(|\vec{r}_1 - \vec{r}_2|, t), \quad (1)$$

$$\rho_{0,2} = n_B^2 X_B(|\vec{r}'_1 - \vec{r}'_2|, t), \quad (2)$$

$$\rho_{1,1} = n_A n_B Y(|\vec{r}_1 - \vec{r}'_1|, t). \quad (3)$$

Thus, we have the first two expressions for similar particle types, $X_\nu(r, t)$, $\nu=A, B$ and a third one for dissimilar particles, $Y(r, t)$, where r is the relative distance between any two particles. These functions describe the spatial distribution of pairs AA , BB , and AB , respectively, and are analogous to the radial distribution function found in statistical physics for systems of dense gases and liquids [23]. These joint correlation functions are normalized to unity as $r \rightarrow \infty$, $X_\nu(\infty, t) = Y(\infty, t) = 1$. The physical meaning of these correlation functions is the following [26,27]:

$$C_A^{(A)}(r, t) = n_A X_A(r, t), \quad (4)$$

$$C_B^{(A)}(r, t) = n_B Y(r, t), \quad (5)$$

where they are mean densities of particles A and B , respectively, at the relative distance r provided that a probe particle A is in the coordinate origin.

The kinetic equations for the many-point densities $\rho_{m,m'}$, taking into account particle creation as well as recombination due to diffusion-controlled reaction $A+B=0$, were found earlier [26,27]. In order to compare results of the mesoscopic and microscopic approaches, we make adjustments here to these equations for the particular problem discussed in above-cited Ref. [20]. That is, we neglect particle creation

and recombination, and the main focus is on the kinetics of system equilibration and on possible pattern formation.

Thus, the number of particles $\rho_{1,0}=n_A$ and $\rho_{0,1}=n_B$ remain constant from now on, and are taken as two system parameters. Among other key parameters are the dynamical interactions between similar and dissimilar particles, $U_{AA}(r)$, $U_{BB}(r)$, and $U_{AB}(r)$, diffusion coefficients denoted by D_A and D_B , and lastly, the temperature T . Even with such simplified system specification, we obtain nontrivial numerical problems which we discuss below.

2. Exact equations of diffusion dynamics

The diffusion dynamic equations are given by [26,27]:

$$\frac{\partial \rho_{m,m'}}{\partial t} = - \sum_{i=1}^m \nabla_i \tilde{J}_{m,m'}^{A,i} - \sum_{j=1}^{m'} \nabla_j' \tilde{J}_{m,m'}^{B,j}, \quad (6)$$

where the diffusion fluxes are

$$\tilde{J}_{m,m'}^{A,i} = -D_A \left(\nabla_i \rho_{m,m'} + \frac{\rho_{m,m'}}{k_B T} \nabla_i W_{m,m'}^i \right), \quad (7)$$

$$\tilde{J}_{m,m'}^{B,j} = -D_B \left(\nabla_j' \rho_{m,m'} + \frac{\rho_{m,m'}}{k_B T} \nabla_j' W_{m,m'}^j \right). \quad (8)$$

Here k_B is the Boltzmann constant, and T is the temperature. In last two expressions for the fluxes, the mean force potential $W_{m,m'}^i$ is introduced, for which

$$\begin{aligned} \nabla_i W_{m,m'}^i &= \sum_{i' \neq i}^m \nabla_{i'} U_{AA}(|\vec{r}_i - \vec{r}_{i'}|) + \sum_{j=1}^{m'} \nabla_j' U_{AB}(|\vec{r}_i - \vec{r}_j'|) \\ &+ \int \frac{\rho_{m+1,m'}}{\rho_{m,m'}} \nabla_i U_{AA}(|\vec{r}_i - \vec{r}_{m+1}|) d\mathbf{r}_{m+1} \\ &+ \int \frac{\rho_{m,m'+1}}{\rho_{m,m'}} \nabla_i U_{AB}(|\vec{r}_i - \vec{r}_{m+1}'|) d\mathbf{r}'_{m+1}. \end{aligned} \quad (9)$$

The potential $W_{m,m'}^j$ is defined similarly. As it is seen from Eq. (9), the mean force acting on a particle A at coordinate \vec{r}_i has both the contribution from *direct* interactions within a group of $(m+m')$ -particles (first two terms in R.H.S.) as well as from *indirect* interactions (integral terms in R.H.S.).

The steady-state (equilibrium) solution of Eq. (6) correspond to setting the fluxes $\tilde{J}_{m,m'}^{A,i}$ and $\tilde{J}_{m,m'}^{B,j}$ to equal zero. The corresponding set of the integro-differential equations coincide *exactly* with the Ivon's equations [23] well known in the statistical physics of dense two-component gases and liquids. As such, Eq. (6) allows us to describe correctly the formation of the equilibrium state in our system. Note that when necessary, these equations could be generalized to take into account possible crystalline structures [34].

3. Structure of the equations

The expression in Eq. (6) for $(m+m')=2$ could be written for the joint correlation functions, and it would contain a diffusion term and drift in the external potential. Thus, the kinetic equation for similar particles reads:

$$\frac{\partial X_\nu(r,t)}{\partial t} = 2D_\nu \nabla \left[\nabla X_\nu(r,t) + \frac{X_\nu(r,t)}{k_B T} \nabla W_\nu(r,t) \right], \quad (10)$$

where $W_\nu(r,t)$ is the mean force potential found in Eq. (9), ($m=2, m'=0$); due to translational invariance and isotropy it has a radial symmetry as similar to the joint correlation functions. According to its definition, the expression in Eq. (9) for the potential $W_\nu(r,t)$ takes into account both direct interactions of similar particles ν (one particle is in the coordinate origin, another at the distance r), and indirect, medium-induced interactions.

The analogous equation for the dissimilar particles follow:

$$\frac{\partial Y(r,t)}{\partial t} = (D_A + D_B) \nabla \left[\nabla Y(r,t) + \frac{Y(r,t)}{k_B T} \nabla W(r,t) \right], \quad (11)$$

However, the mean force potential $W(r,t)$ here becomes more complicated:

$$W(r,t) = \frac{D_A}{D_A + D_B} W_{AB} + \frac{D_B}{D_A + D_B} W_{BA}. \quad (12)$$

The potential W_{AB} corresponds to the particle configuration where A is in the origin and B separated by the distance r , whereas the potential W_{BA} indicates the location exchange for particles A and B . In both cases, the integral terms in Eq. (9) with $m=1, m'=1$ describe indirect particle interactions through medium.

The set of equations found in Eq. (6) is obviously not closed since the mean force potentials are defined through the many-particle densities $\rho_{m,m'}$ ($m+m' > 2$). It is common in the condensed matter physics to decouple such infinite equation sets using some approximations. We will restrict ourselves here to the binary approximation corresponding to the closed set of the kinetic equations for the joint correlation functions over similar and dissimilar particle types.

In fact, we used two approximations. First, our theory is based on the Kirkwood superposition approximation for three-particle densities [23,35] and the self-consistent treatment of the electrostatic interactions defined by the nonuniform spatial distribution of similar and dissimilar particle types. In our formulation, the pair potential contains two independent contributions:

$$U_{\nu\nu'}(r) = U_{\nu\nu'}^{LJ}(r) + U_{\nu\nu'}^C(r). \quad (13)$$

The former potential is a short-range van der Waals interaction, which is described, following [20], in terms of a classic 6–12 Lennard-Jones (LJ) potential

$$U_{\nu\nu'}^{LJ}(r) = 4U_0 \left[\left(\frac{r_0}{r} \right)^{12} - \left(\frac{r_0}{r} \right)^6 + C_{\nu\nu'} \right]. \quad (14)$$

The parameter U_0 is the same for both the similar and dissimilar particles. However, the condition $C_{\nu\nu}=0$ applies for similar particles, whereas for dissimilar particles the interaction potential is shifted up, as $C_{AB}=1/4$, and cut at $r_c = 2^{1/6}r_0$, where r_0 is an effective molecular radius.

The second term in the potential is the long-range Coulomb interaction,

$$U_{\nu\nu'}^C(r) = \frac{e_\nu e_{\nu'}}{\epsilon r}, \quad (15)$$

where ϵ is the dielectric constant.

The mean force potentials could be similarly split into two contributions, e.g., $W_A(r, t) = W_A^L(r, t) + W_A^C(r, t)$. The technical details of the mean force potential calculations are summarized in the Appendix A.

Choice of the partial diffusion coefficients D_A and D_B depends on a particular physical system. For instance, for radiation-induced defects in most solids pairs A , B of complementary (Frenkel) defects (interstitial atom-vacancy) are created whose mobilities strongly differ [26,27]. Obviously, very different situations could occur for molecules at interfaces. If proteins diffuse on a surface their diffusion constant will depend on the degree of hydrophobicity [36], $D \approx 10^{-7}$ cm²/s. For simplicity, in this paper we assume equal diffusion coefficients, $D_A = D_B$, whereas asymmetry in molecule mobilities will be discussed in a separate paper.

4. Parameterization

Let us use henceforth the dimensionless units as follows: the length in units r_0 defining the Lennard-Jones potential, so that the total particle density, denoted by $n = n_A + n_B$, determines the dimensionless parameter $\eta = nr_0^2$. The time unit is $\tau = r_0^2 / (D_A + D_B)$, and the dimensionless temperature is $\theta = T/T_0$, where $T_0 = U_0/k_B$ is defined by the U_0 entering the Lennard-Jones potential. The relative contribution of the Coulomb potential with respect to the Lennard-Jones potential is characterized by $\delta = e^2 / \epsilon r_0 k_B T_0$. The asymmetry in the particle diffusion coefficients is described by the parameter $\mu = D_A / (D_A + D_B)$. As the initial particle distribution we will use the random (Poisson) one, with $X_\nu(r, 0) = Y(r, 0) = 0$ for $r \leq r_0$, but $X_\nu(r, 0) = Y(r, 0) = 1$ as $r > r_0$. Deviation of the correlation functions above (and below) the unity value indicates the enrichment (or depletion) of the concentration with respect to the random distribution. As such, this permits us a way to characterize the particle aggregation. To summarize, the diffusion-controlled process is controlled by the following set of four parameters: $(\eta, \theta, \delta, \mu)$.

B. Reverse Monte Carlo method

1. Modeling algorithm

The RMC technique was proposed in Refs. [28–30], in order to generate particle configurations that are consistent with experimentally measured radial distribution functions or the structure factors. Although at first RMC was designed for liquid and glassy materials, it was also later applied to crystalline systems [37] as well. A review of RMC applications is given in Refs. [38,39]. An advantage of the RMC method is based on the fact that no interatomic forces or atomic potentials are used in the process [38]. The RMC is most useful for spherically symmetric pair potential obtained from an experimentally observed structure factors or pair correlation functions. There are other recent inverse techniques that can

incorporate more information than the pair correlation function, which are useful for interaction potential that are not necessarily pairwise additive or spherically symmetric [40] or for materials transparent to specific wavelengths of radiation [41].

The RMC approach is based on the goodness-of-fit statistical model, for example, by using the Pearson χ^2 test [43]. The value of this test-statistics is

$$\chi^2 = \sum_{i=1}^n \frac{(O_i - O_i^0)^2}{O_i^0}, \quad (16)$$

where O_i is an observed frequency, O_i^0 an expected (standard) frequency, and n the number of fitting parameters. The resulting value can be compared to the χ^2 distribution, to determine the goodness-of-fit. (It is assume that both O_i and O_i^0 are positively defined, otherwise other tests should be considered [28–30]). In the standard RMC the expected frequency O_i^0 is usually taken from experimental data, as for example, the pair distribution function and its Fourier transform, the latter is typically derived directly from neutron or x-ray total scattering data. These data should be fitted using the Monte Carlo method. The observed frequency O_i is a result of computer modeling of a random process. An initial configuration in Monte Carlo method is constructed by placing N_A and N_B atoms in a periodic boundary cell, and measurable quantities O_i are calculated for a given atomic configuration. By moving atoms in the system and recalculating the χ^2 , one strives to reproduce the standard data. There exist different algorithms of systematic reduction of the χ^2 value. A more difficult problem is to make this procedure fast and efficient for practical applications. In our case, the standard data O_i^0 are the pair distribution functions which are solutions of the above-considered set of integro-differential equations. In the numerical solution a small enough coordinate increment $\Delta r = r_0/40$ is used. We next discuss the procedure for the calculations of the standard data O_i^0 .

The solution of nonlinear diffusion equations describing particle drift in the external field yields for a given time t the particle coordinates $r_i = i\Delta r$, $i = 1, 2, \dots$. Each coordinate r_i is associated with three joint correlation functions, $X_A(r_i, t)$, $X_B(r_i, t)$, $Y(r_i, t)$. Each of these functions is positive, $X_A(r_i, t)$, $X_B(r_i, t)$, $Y(r_i, t) > 0$ and vanishes for the coordinate region corresponding to the finite size of the particles. This permits us to use in the RMC the effective choice of the so-called cost function [42], based on the idea of the χ^2 test of Pearson [43].

Using the RMC method, we compare the analytically calculated correlation functions with the MC simulations. We consider the periodic 2D system characterized by the square $S = L^2$. The discrete choice of the particle coordinates in numerical calculations suggests the consideration of concentric rings with the square $s_i = 2\pi \int_{r_i - \Delta r/2}^{r_i + \Delta r/2} r dr \approx 2\pi r_i \Delta r$.

If we draw such rings for all particles A and calculate the number of particles B in these rings, this procedure would give us the number of N_i^{AB} pairs separated by the relative distance $r \in [r_i - \Delta r/2, r_i + \Delta r/2]$. In the limit $L \rightarrow \infty$ this gives us the correlation function

$$Y(r_i, t) = \frac{N_i^{AB}}{Ss_i n_A n_B}. \quad (17)$$

Using the correlation function for a finite-size system, one can define the *standard* number of AB pairs

$$\bar{N}_i^{AB} = Y(r_i, t) Ss_i n_A n_B, \quad (18)$$

as well as AA pairs:

$$\bar{N}_i^{AA} = X_A(r_i, t) Ss_i n_A n_A / 2. \quad (19)$$

The quantities \bar{N}_i^{AB} , \bar{N}_i^{AA} , \bar{N}_i^{BB} serve as standard data O_i^0 whereas N_i^{AB} , N_i^{AA} , N_i^{BB} are observed data O_i being obtained from the Monte Carlo simulations.

2. χ^2 goodness-of-fit test

As mentioned above, the χ^2 -goodness-of-fit test (of Pearson) [43] is defined using the statistics for a random variable

$$Z = \sum_i^{i_{\max}} \left[\frac{(N_i^{AA} - \bar{N}_i^{AA})^2}{\bar{N}_i^{AA}} + \frac{(N_i^{BB} - \bar{N}_i^{BB})^2}{\bar{N}_i^{BB}} + \frac{(N_i^{AB} - \bar{N}_i^{AB})^2}{\bar{N}_i^{AB}} \right]. \quad (20)$$

Using the RMC, one has to decrease systematically the value of a random variable Z .

When a randomly selected particle moves to a new trial position, the function Z' is recalculated. If the cost function Z' has decreased, this step is accepted. In contrast, when $Z' > Z$, the step is rejected in our algorithm (as in the Metropolis algorithm [44]).

As $L \rightarrow \infty$ (i.e., an increase in a number of particle pairs), the Z distribution should approach the χ^2 -distribution with approximately $m \approx 3i_{\max}$ degrees of freedom [43]. An essential condition is that any standard variable in Eq. (20) for large enough Z , \bar{N}_i^{AA} , \bar{N}_i^{BB} , $\bar{N}_i^{AB} \gg 10$. This condition could be fulfilled by an increase of the system size. A potential problem that might arise is related to small coordinate areas that correspond to the finite molecular size accounted for in the LJ potentials. The fact that there exists no pairs for which the relative distances are smaller than the molecule diameter could be taken into account through additional boundary conditions imposed in the modeling; we have introduced here a hard-sphere model in order to avoid the atoms getting too close to each other.

III. RESULTS

The kinetic problem that we discuss has four free *control* parameters—(η , θ , δ , μ)—the elucidation of which needs further detailed analysis in future works. The main purpose of this paper is to demonstrate the applicability of the aforementioned method using several typical examples.

One of the main characteristics obtained from the numerical solution for the set of nonlinear equations is the joint correlation functions at a given time t as shown in Fig. 1. It can be seen how a random, disordered mixture of molecules in the beginning can change with time to a structure with well-defined short and intermediate order. (Note that we use

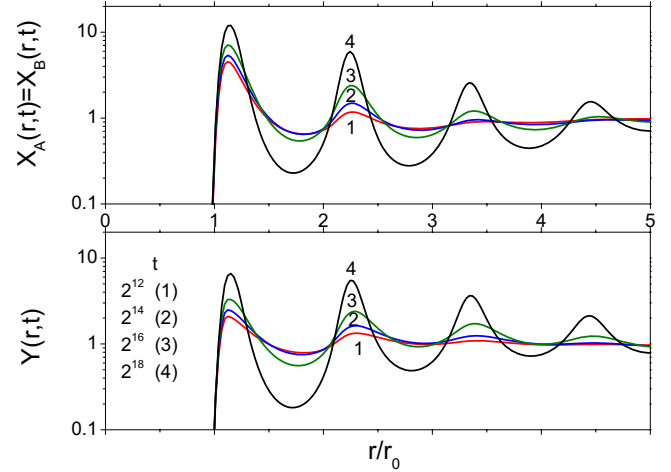


FIG. 1. (Color online) The correlation functions calculated for parameter set $\eta=0.4$, $\theta=0.35$, $\delta=0.35$, and $\mu=0.5$; the observation time t : (1) 2^{12} , (2) 2^{14} , (3) 2^{16} , and (4) 2^{18} .

time units $\tau = r_0^2 / (D_A + D_B)$ and the logarithmic scale in plotting the correlation functions). This structure corresponds to a mixture of the dense molecular packing (condensed phase) and loosely populated areas (a gas phase). These correlation functions will be used later for detailed system characterization, such as nonequilibrium charge screening and deviation from the Debye-Huckel theory, as well as the structural factors using the Fourier transforms.

However, the relationship between the calculated joint correlation functions and the molecular structure in a real space is not obvious and far from trivial, since we are dealing here with the nonequilibrium mixture of condensed and gas phases. To visualize the system structure, we use the aforementioned RMC method.

The high quality of the RMC is obvious in Fig. 2 where the analytically calculated *standard* correlation functions (full lines) practically coincide with those (circles) obtained using the RMC for modeling our spatial structures. The small fractions of the relevant snapshots are shown in Fig. 3. Thus, we obtain Fig. 3 with structure snapshots from the analysis of the correlation functions in Fig. 1 for the same time moments in a wide temporal range. To illustrate RMC convergence, the black circles in window (d) show the results for a small number of MC steps, while open circles correspond to a large number of MC steps. We note that the ratio of the number of the MC steps is very large at 256.

In Fig. 2, the cases of a) to c) correspond to the disordered (liquid-like) structures where the RMC can be applied very efficiently. Increasing the systems size, one can always suppress the fluctuations in the system. Consequently, the RMC correlation functions are as smooth as those obtained using the numerical solution of the kinetic equations. The convergence is also very good, as demonstrated by the coincidence of the black and open circles in windows (a) to (c) (the black symbols are not shown here for clarity).

In Fig. 2(d), we show results corresponding to the longest-time system evolution. Despite the increase in the number of MC steps, there is slight improvement in the agreement between the RMC and standard correlation func-

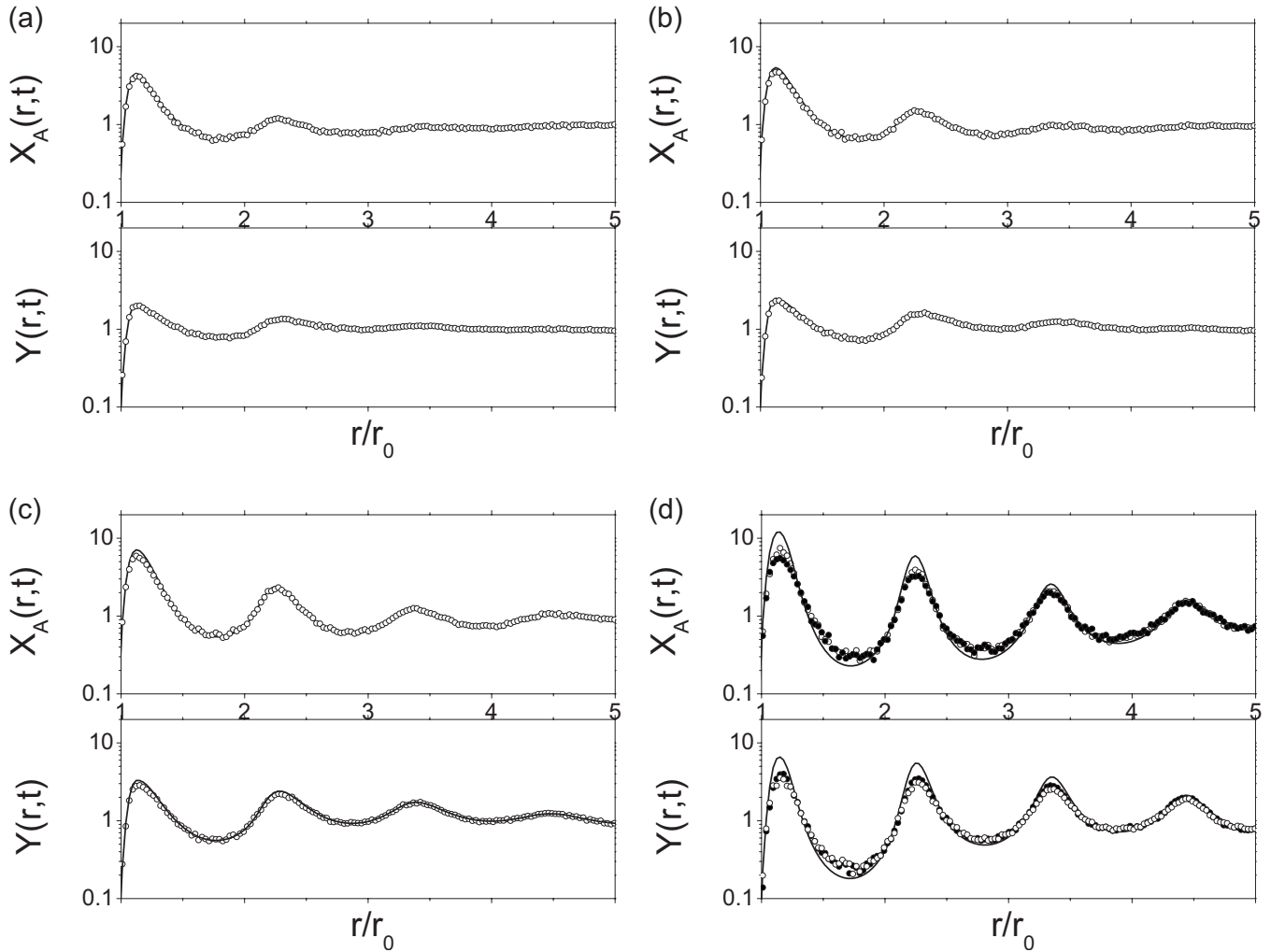


FIG. 2. The calculated correlation functions (full curves), and their RMC approximation (circles). The time t : (a) 2^{12} , (b) 2^{14} , (c) 2^{16} , and (d) 2^{18} . Parameters: $\eta=0.4$, $\theta=0.35$, $\delta=0.35$, and $\mu=0.5$.

tions (black and open circles); in fact, a considerable discrepancy is observed for the first maximum and minimum for the similar-molecule correlation functions $X_A(r, t)$. The reason of limited applicability of RMC in this regime could be understood from the analysis of snapshots in Figs. 3(c) and 3(d). One can see here the formation of a dense structure with considerable ordering typical for crystals, and the distances between nearest molecules become very similar with small fluctuations. Therefore, large fluctuations in molecular positions typical for liquids are strongly suppressed here.

This is supported also by the analysis of the correlation functions shown in Fig. 1 for similar-type molecules at long simulation times: the first maximum monotonically increases and first minimum decreases, so that their ratio reaches a factor of about 100. (Remember the logarithmic scale used in Fig. 1.) The numerical analysis shows also that, at long simulation times, the amplitudes of first maxima are ill-defined and depend on the coordinate increment used in the difference equations. A similar problem is well known for modeling the discrete lattice using a set of Dirac δ -functions. In other words, the singularities in Fig. 1 arise due to formation of dense ordered structures (local crystallization). The probability to obtain such structures using the random molecule

permutations used in the RMC is extremely low, and this is a main reason why this method fails for the ordered structure phases. Thus, the snapshots in Fig. 3(d) only yield a qualitative idea on the underlying atomic structure. Alongside with the RMC, we can use other pattern characterization methods, such as the analysis of the non-equilibrium charge screening to be discussed in a forthcoming paper. Note that the ordering and disordering is again controlled by the four above-mentioned parameters—($\eta, \theta, \delta, \mu$).

IV. CONCLUSIONS

In this paper, the analytical formalism of joint correlation functions and the reverse Monte Carlo are combined to visualize pattern formation in processes tending toward equilibrium for systems containing two kinds of oppositely charged molecules adsorbed at a surface or at an interface. We provide illustrations that demonstrate the method's ability in different situations. The analysis of the segregation of various components into clusters of charges done here is an alternative approach to the standard kinetic Monte Carlo or molecular dynamics simulations. The method is based on computing radial distribution functions by solving a set of

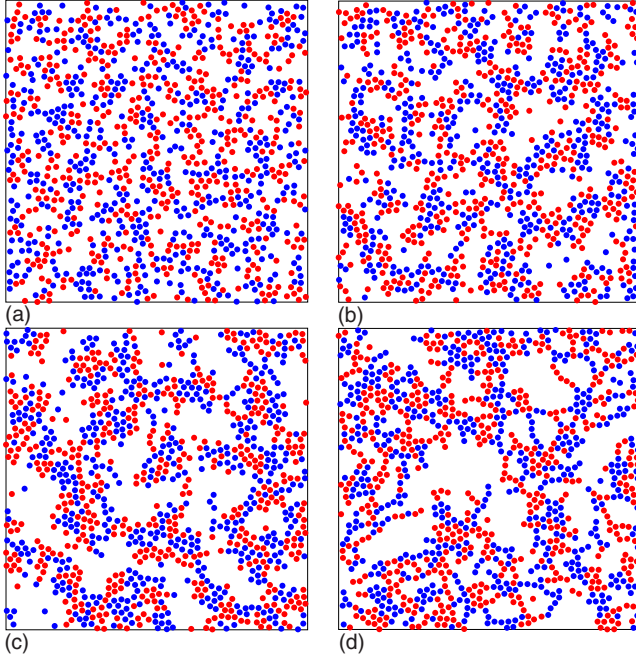


FIG. 3. (Color online) Fragments of the characteristic snapshots obtained using the RMC for the correlation functions in Fig. 2. The snapshots numbering corresponds to (a)-(d) in Fig. 2. Parameters: $\eta=0.4$, $\theta=0.35$, $\delta=0.35$, and $\mu=0.5$.

nonlinear equations, and obtaining spatial configurations of the molecules that best fit these computed radial functions via the reverse Monte Carlo method. The formalism is suitable for systems with intermediate order such as dense gases, liquids or amorphous solids. The joint correlation functions, obtained numerically from the set of nonlinear equations, show a disordered mixture that changes with time. They initially form clusters of rather dense molecular packing (condensed phase) coexisting with loosely populated areas (a gas phase). Then, the free charged molecules (in the gas phase) form chains of like-charged molecules that connect the different denser clusters forming a rather unusual percolated structure. Interestingly, computer simulations of the restricted primitive model (RPM) (i.e., without short range van der Waals attractions among the components) for oppositely charged spheres have demonstrated the formation of chains via dimers [48]. Furthermore, the number of free ions in this model at the critical temperature is nearly zero [49]. Phase coexistence of the charged hard dumbbell (CHD) system is found to be very close to that of the RPM [31,50–53] and theory yields the best results when ions are assumed to be fully paired [54]. In our model, we find chainlike structures as the time evolves but of the same sign; this is due to the competing interactions since van der Waals forces induce attraction among same-sign molecules and the electrostatic force repulsions. The structures look similar to the structures found in co-assembled oppositely charged nanoparticles on surfaces, which can be ordered using AC fields [21]. We can explore a broad range of phenomena of electrostatics at the nanoscale with our numerical method. A further advantage of our model, over classical Monte Carlo, is the information regarding the nonequilibrium states during the segregation process.

ACKNOWLEDGMENTS

This work was supported by the Nonequilibrium Energy Research Center (NERC) which is an Energy Frontier Research Center funded by the U.S. Department of Energy, Office of Science, Office of Basic Energy Sciences under Award No. DE-SC0000989, and by ESF under Grant No. 2009/0202/1DP/1.1.1.2.0/09/APIA/VIAA/141 (G.Z.). We thank William Kung for his useful comments.

APPENDIX A: CALCULATIONS OF THE MEAN FORCE POTENTIALS

In order to calculate the Lennard-Jones potential contribution into a mean force potential in Eq. (9), we use the Kirkwood superposition approximation. This reduces the three-particle densities to a product of two-particle densities. In particular, for $\rho_{2,1}=\rho_{2,1}(\vec{r}_1, \vec{r}_2; \vec{r}'_1; t)$ we use the approximation

$$\rho_{2,1} \Rightarrow n_A^2 n_B X_A(|\vec{r}_1 - \vec{r}_2|, t) Y(|\vec{r}_1 - \vec{r}'_1|, t) Y(|\vec{r}_2 - \vec{r}'_1|, t). \quad (\text{A1})$$

As a result, we arrive at the following (differential) expression for the mean force potentials [27]:

$$\begin{aligned} \nabla W_A^{LJ}(r, t) = & \nabla U_{AA}^{LJ}(r) + n_A \int \nabla U_{AA}^{LJ}(r'') X_A(r'', t) X_A(r', t) d\mathbf{r}' \\ & + n_B \int \nabla U_{AB}^{LJ}(r'') Y(r'', t) Y(r', t) d\mathbf{r}', \end{aligned} \quad (\text{A2})$$

$$\begin{aligned} \nabla W_B^{LJ}(r, t) = & \nabla U_{BB}^{LJ}(r) + n_B \int \nabla U_{BB}^{LJ}(r'') X_B(r'', t) X_B(r', t) d\mathbf{r}' \\ & + n_A \int \nabla U_{AB}^{LJ}(r'') Y(r'', t) Y(r', t) d\mathbf{r}', \end{aligned} \quad (\text{A3})$$

$$\begin{aligned} \nabla W_{AB}^{LJ}(r, t) = & \nabla U_{AB}^{LJ}(r) + n_A \int \nabla U_{AA}^{LJ}(r'') X_A(r'', t) Y(r', t) d\mathbf{r}' \\ & + n_B \int \nabla U_{AB}^{LJ}(r'') Y(r'', t) X_B(r', t) d\mathbf{r}', \end{aligned} \quad (\text{A4})$$

where the relative coordinate is $\mathbf{r}'' = \mathbf{r} - \mathbf{r}'$.

Second, the treatment of the long-range Coulomb potential requires the use of another idea discussed earlier [45–47]. This is based on the definition of the joint correlation functions having a very clear and transparent physical meaning. Thus, for a probe particle of the type A in the origin of the coordinate system, the functions $C_A^{(A)}(r, t)$ and $C_B^{(A)}(r, t)$, Eqs. (4) and (5), give the average concentrations of similar or dissimilar particles at a distance r from the origin. This is why

$$\sigma_A(r, t) = e_A n_A X_A(r, t) + e_B n_B Y(r, t) \quad (\text{A5})$$

can be interpreted as the mean *charge density* induced by a probe charge A in the coordinate origin. This quantity is used below in the calculation of the effective potentials in the spirit of the Debye-Hückel theory [23]. We use also standard

assumption that the system is electrically neutral:

$$n_A e_A + n_B e_B \equiv 0, \quad (\text{A6})$$

where e_A, e_B are molecule charges.

Let us start with the Poisson equation (in its integral form) for the potential produced by a probe charge in $3d$ A

$$\varphi_A(x, y, z, t) = \frac{e_A}{\epsilon r} + \int \frac{\rho_A(\mathbf{r}', t) dx' dy' dz'}{\epsilon |\mathbf{r} - \mathbf{r}'|}. \quad (\text{A7})$$

Here ρ_v is the density of induced charge. Assume now that the surface process under study occurs in the x, y plane ($2d$). In this case we are interested only in the potential at $z=0$, $\phi_A(r, t) = \varphi_A(x, y, z=0, t)$ with $r = \sqrt{x^2 + y^2}$. It can be obtained from Eq. (A7) with the evident substitution, $\rho_A(x, y, z, t) = \sigma_A(r, t) \delta(z)$, where δ is the Dirac delta-function and using the radial symmetry.

Using the neutrality condition, Eq. (A6), we obtain the following integral relation

$$\phi_A(r, t) = \frac{e_A}{\epsilon r} + \frac{e_A n_A}{\epsilon} \int \frac{[X_A(r', t) - Y(r', t)] dx' dy'}{|\mathbf{r} - \mathbf{r}'|}, \quad (\text{A8})$$

This relation permits to calculate the mean force potentials for molecular pairs in the framework of the Debye-Hückel theory:

$$W_A^C(r, t) = e_A \phi_A(r, t), W_B^C(r, t) = e_B \phi_B(r, t), \quad (\text{A9})$$

$$W_{AB}^C(r, t) = e_B \phi_A(r, t), W_{BA}^C(r, t) = e_A \phi_B(r, t). \quad (\text{A10})$$

APPENDIX B: NUMERICAL METHODS

There are two problems in the numerical solution of our non-linear differential equations: (i) mean force potentials (both Lennard-Jones and Coulomb) contain double integrals which calculations are time consuming, and (ii) mean force potentials have a singularity as $r \rightarrow 0$, and change sharply near r_0 . Using analytical transformations, the double integrals can be reduced to two ordinary integrals. In particular, let us use the polar coordinate system when calculating the Coulomb potential in the integral relation, Eq. (A8)

$$\int \frac{\sigma_v(r', t) dx' dy'}{|\mathbf{r} - \mathbf{r}'|} = 2\pi \int_0^\infty \sigma_v(r', t) r' \frac{dK(r, r')}{dr'} dr'. \quad (\text{B1})$$

This is now a one-dimensional integral which needs however preliminary accurate calculation of the integral kernel

$$\begin{aligned} K(r, r') &\equiv K(z) \\ &= \frac{1}{\pi} \int_0^\pi d\vartheta [\sqrt{1 - 2z \cos \vartheta + z^2} \\ &\quad + \cos \vartheta \ln |2\sqrt{1 - 2z \cos \vartheta + z^2} + 2z - 2 \cos \vartheta|], \end{aligned} \quad (\text{B2})$$

where $z = r'/r$.

Therefore, after calculating this expression with the necessary accuracy, the integral Eq. (B1) can be calculated by

means of a standard trapezoid method. The calculation of the Lennard-Jones potentials is more time consuming since the integral kernels here depend on the correlation functions and cannot be preliminary calculated as in the case of the Coulomb potential.

The cutoff introduced at r_c in Eq. (14) makes the Lennard-Jones potential nondifferentiable at short distances. However, this fact makes no problems since Eqs. (A2)–(A4) instead of mean field potentials $W(r, t)$ contain their derivatives $dW(r, t)/dr$, thus the potential step change is easily taken into account in the discrete difference scheme used in solving the equations. To avoid this potential step, one has to introduce additional parameters which we tried to avoid.

The main problem arises due to the necessity of solving nonlinear, partial differential equations with singular potentials. To illustrate our method of their solution, consider the typical equation

$$\partial g(r, t) / \partial t = r^{-1} \partial [rj(r, t)] / \partial r, \quad (\text{B3})$$

$$j(r, t) = \partial g(r, t) / \partial r + \partial W[g, r, t] / \partial r g(r, t). \quad (\text{B4})$$

Here $W[g, r, t]$ are functionals of $g(r, t)$ sought for and $W[g, r, t]$ has a singularity in r : $W[g, r, t] = \infty$ as $r \rightarrow 0$. After the discretization of the equation using a standard method, $r_i = i\Delta r$, $t_m = m\Delta t$, $g(r_i, t_m) = g_i^0$, $g(r_i, t_{m+1}) = g_i$, we arrive at the difference equation which could be presented in a quasilinearized traditional form

$$a_i [\bar{g}] g_{i-1} + b_i [\bar{g}] g_{i+1} - c_i [\bar{g}] g_i - g_i / \Delta t = -g_i^0 / \Delta t, \quad (\text{B5})$$

where coefficients a_i, b_i, c_i arise due to the approximation of $r^{-1} \partial [rj(r, t)] / \partial r$. These coefficients depend on $W[g, r, t]$ and, thus, are functionals of g . Solution of Eq. (B3) is obtained by means of quasi-linearization: $\bar{g}_i = g_i^0$ is used as initial guess, Eq. (B3) is solved in the standard way, then we substitute $\bar{g}_i = g_i$ and the iterative process continues until convergence is achieved within a required tolerance. In this way, we avoid a problem of the nonlinearity of the kinetic equations.

The approximation of $r^{-1} \partial [rj(r, t)] / \partial r$ is less trivial. Use of finite differences for derivatives fails for the singular potentials since negative coefficients a_i or b_i become so large that this cannot be compensated by any reduction of the time increment, Δt . We suggested the procedure where always $a_i, b_i, c_i \geq 0$. This allows to perform calculations for sufficiently large Δt values. Similar procedure was discussed earlier [47] in the one-dimensional case with the singular potential.

The procedure is as follows. To obtain a *conservative* difference scheme, one integrates the initial differential equation in the cylindrical layer in the interval r in $[r_{i-1/2}, r_{i+1/2}]$ with $r_{i\pm 1/2} = (i \pm 1/2)\Delta r$. The problematic term reads now

$$\int (r^{-1} \partial [rj(r, t)] / \partial r) r dr = r_{i+1/2} j_{i+1/2} - r_{i-1/2} j_{i-1/2}. \quad (\text{B6})$$

In the equation for the flux density, $j = \partial g / \partial r + (\partial W / \partial r) g$, substitution $g = \exp(-W) \omega$ gives $j = (\partial \omega / \partial r) \exp(-W)$. It is important that the exponent, $\exp(W)$, has the argument W rapidly changing on the scale Δr and thus also changes rapidly as compared to the slowly varying functions j and

$\partial W/\partial r$. This is why the integral in the interval $r \in [r_{i-1}, r_i]$

$$\int j \exp(W) dr = \omega_i - \omega_{i-1} \quad (\text{B7})$$

could be estimated as

$$\begin{aligned} \int j \exp(W) dr &\approx j_{i-1/2}/(\partial W/\partial r)_{i-1/2} \int \exp(W) dW \\ &= j_{i-1/2}/(\partial W/\partial r)_{i-1/2} [\exp(W_i) - \exp(W_{i-1})] \\ &\approx j_{i-1/2} \frac{[\exp(W_i) - \exp(W_{i-1})]}{(W_i - W_{i-1})} \Delta r. \end{aligned} \quad (\text{B8})$$

Now returning from the intermediate function ω to g sought for, one obtains the basic relation for the difference scheme coefficients

$$j_{i-1/2} = (g_i \exp(\Delta W_i) - g_{i-1}) \frac{\Delta W_i/\Delta r}{\exp(\Delta W_i) - 1}, \quad (\text{B9})$$

where $\Delta W_i = W_i - W_{i-1}$. As it should be, the flux density depends not on the very potential W but on its derivative. The obtained approximation, Eq. (B8), is then used in Eq. (B6) to calculate the coefficients a_i, b_i, c_i in the difference scheme, Eq. (B5).

-
- [1] R. Ogaki, M. Alexander, and P. Kingshott, *Mater. Today* **13**, 22 (2010).
- [2] H. Zhang, Z. Li, and C. A. Mirkin, *Adv. Mater.* **14**, 1472 (2002); J. C. Smith *et al.*, *Nano Lett.* **3**, 883 (2003).
- [3] M. Bier, J. de Graaf, J. Zwanikken, and R. van Roij, *J. Chem. Phys.* **130**, 024703 (2009).
- [4] W. Kung, F. Solis, and M. Olvera de la Cruz, *J. Chem. Phys.* **130**, 044502 (2009).
- [5] Z. G. Wang, *Phys. Rev. E* **81**, 021501 (2010).
- [6] M. Tagliazucchi, M. Olvera de la Cruz, and I. Szleifer, *Proc. Natl. Acad. Sci. U.S.A.* **107**, 5300 (2010).
- [7] A. Travesset and S. Vangaveti, *J. Chem. Phys.* **131**, 185102 (2009).
- [8] M. Olvera de la Cruz, *Soft Matter* **4**, 1735 (2008).
- [9] D. L. Wilson *et al.*, *PNAS* **98**, 13660 (2001); Y. S. Velichko and M. Olvera de la Cruz, *Phys. Rev. E* **72**, 041920 (2005); K. L. Kohlstedt, F. J. Solis, G. Vernizzi, and M. O. de la Cruz, *Phys. Rev. Lett.* **99**, 030602 (2007); G. Vernizzi, K. L. Kohlstedt, and M. Olvera de la Cruz, *Soft Matter* **5**, 736 (2009).
- [10] M. Dubois, B. Deme, T. Gulik-Krzywicki, J. C. Dedieu, C. Vautrin, S. Desert, E. Perez, and T. Zemb, *Nature (London)* **411**, 672 (2001); G. Vernizzi and M. Olvera de la Cruz, *PNAS* **104**, 18382 (2007); M. A. Greenfield *et al.*, *J. Am. Chem. Soc.* **131**, 12030 (2009).
- [11] F. J. Solis, S. I. Stupp, and M. Olvera de la Cruz, *J. Chem. Phys.* **122**, 054905 (2005); R. Parthasarathy, P. A. Cripe, and J. T. Groves, *Phys. Rev. Lett.* **95**, 048101 (2005); S. M. Loverde *et al.*, *J. Chem. Phys.* **124**, 144702 (2006); S. M. Loverde and M. Olvera de la Cruz, *ibid.* **127**, 164707 (2007); A. Naydenov, P. A. Pincus, and S. A. Safran, *Langmuir* **23**, 12016 (2007).
- [12] I. Lagzi, B. Kowalczyk, and B. A. Grzybowski, *J. Am. Chem. Soc.* **132**, 58 (2010).
- [13] E. E. Meyer, Q. Lin, T. Hassenkam, E. Oroudjev, and J. N. Israelachvili, *PNAS* **102**, 6839 (2005); Y. S. Velichko and M. Olvera de la Cruz, *J. Chem. Phys.* **124**, 214705 (2006).
- [14] A. D. Stoycheva and S. J. Singer, *Phys. Rev. E* **64**, 016118 (2001).
- [15] O. Hellwig, A. Berger, and E. E. Fullerton, *Phys. Rev. B* **75**, 134416 (2007).
- [16] M. Sayar, M. Olvera de la Cruz, and S. I. Stupp, *EPL* **61**, 334 (2003).
- [17] M. Park, P. M. Chaikin, R. A. Register, and D. H. Adamson, *Appl. Phys. Lett.* **79**, 257 (2001); S. O. Kim, H. H. Solak, M. P. Stoykovich, N. J. Ferrier, J. J. de Pablo, and P. F. Nealey, *Nature (London)* **424**, 411 (2003).
- [18] Y. De Decker, H. Marbach, M. Hinz, S. Günther, M. Kiskinova, A. S. Mikhailov, and R. Imbihl, *Phys. Rev. Lett.* **92**, 198305 (2004).
- [19] A. D. Stroock, M. Weck, D. T. Chiu, W. T. S. Huck, P. J. A. Kenis, R. F. Ismagilov, and G. M. Whitesides, *Phys. Rev. Lett.* **84**, 3314 (2000); Y. S. Velichko, F. J. Solis, and M. Olvera de la Cruz, *J. Chem. Phys.* **128**, 144706 (2008); E. Petersen, B. Q. Li, F. X. Fang, H. B. Luo, V. Samuilov, D. Gersappe, J. Sokolov, B. Chu, and M. Rafailovich, *Phys. Rev. Lett.* **98**, 088102 (2007).
- [20] S. M. Loverde, F. J. Solis, and M. Olvera de la Cruz, *Phys. Rev. Lett.* **98**, 237802 (2007).
- [21] M.-G. Song, K. J. M. Bishop, A. O. Pinchuk, B. Kowalczyk, and B. A. Grzybowski, *J. Phys. Chem. C* **114**, 8800 (2010).
- [22] T. Okuzono and T. Ohta, *Phys. Rev. E* **67**, 056211 (2003).
- [23] R. Balescu, *Equilibrium and Non-equilibrium Statistical Mechanics* (Wiley, New York, 1975).
- [24] Focus Issue, *The Fermi-Pasta-Ulam Problem. The First Fifty Years*, edited by D. K. Campbell, P. Rosenau, and G. M. Zaslavsky, *Chaos* **15** (2005).
- [25] G. P. Berman and F. M. Izrailev, *Chaos* **15**, 015104 (2005).
- [26] E. A. Kotomin and V. N. Kuzovkov, *Rep. Prog. Phys.* **55**, 2079 (1992).
- [27] E. A. Kotomin and V. N. Kuzovkov, *Modern Aspects of Diffusion-Controlled Reactions: Cooperative Phenomena in Bimolecular Processes, Vol. 34 of Comprehensive Chemical Kinetics* (Elsevier, North Holland, Amsterdam, 1996).
- [28] R. L. McGreevy and L. Pusztai, *Mol. Simul.* **1**, 359 (1988).
- [29] R. L. McGreevy, *Nucl. Instrum. Methods Phys. Res. A* **354**, 1 (1995).
- [30] R. L. McGreevy, *J. Phys.: Condens. Matter* **13**, R877 (2001).
- [31] J. M. Romero-Enrique, G. Orkoulas, A. Z. Panagiotopoulos, and M. E. Fisher, *Phys. Rev. Lett.* **85**, 4558 (2000).
- [32] Q. Yan and J. J. de Pablo, *Phys. Rev. Lett.* **88**, 095504 (2002); **86**, 2054 (2001).
- [33] V. N. Kuzovkov and E. A. Kotomin, *Rep. Prog. Phys.* **51**, 1479 (1988).
- [34] V. N. Kuzovkov, E. A. Kotomin, and W. von Niessen, *Phys. Rev. B* **58**, 8454 (1998).

- [35] J. G. Kirkwood, *J. Chem. Phys.* **3**, 300 (1935).
- [36] J. J. Ramsden, *J. Phys. Chem.* **96**, 3388 (1992).
- [37] M. G. Tucker, M. T. Dove, and D. A. Keen, *J. Appl. Crystallogr.* **34**, 630 (2001).
- [38] J. C. de Lima, D. Raoux, Y. Charriere, and M. Maurer, *J. Phys.: Condens. Matter* **20**, 115103 (2008).
- [39] M. G. Tucker, M. T. Dove, and D. A. Keen, in *Total Scattering and Reverse Monte Carlo Modeling of Disordered Crystalline Materials From Semiconductors to Proteins: Beyond the Average Structure*, edited by S. J. L. Billinge and M. F. Thorpe (Springer, New York, 2002), pp. 85–103.
- [40] S. Torquato, *Soft Matter* **5**, 1157 (2009).
- [41] R. D. Batten, F. H. Stillinger, and S. Torquato, *J. Appl. Phys.* **104**, 033504 (2008).
- [42] P. Biswas, R. Atta-Fynn, and D. A. Drabold, *Phys. Rev. B* **69**, 195207 (2004).
- [43] P. E. Greenwood and M. S. Nikulin, *A Guide to Chi-Squared Testing* (Wiley, New York, 1996).
- [44] N. Metropolis, A. W. Rosenbluth, M. N. Rosenbluth, A. H. Teller, and E. Teller, *J. Chem. Phys.* **21**, 1087 (1953).
- [45] V. N. Kuzovkov and E. A. Kotomin, *Chem. Phys.* **98**, 351 (1985).
- [46] V. N. Kuzovkov, E. A. Kotomin, and W. von Niessen, *J. Chem. Phys.* **105**, 9486 (1996).
- [47] V. N. Kuzovkov, E. A. Kotomin, and W. von Niessen, *Phys. Rev. E* **54**, 6128 (1996).
- [48] J. M. Romero-Enrique, L. F. Rull, and A. Z. Panagiotopoulos, *Phys. Rev. E* **66**, 041204 (2002).
- [49] P. J. Camp and G. N. Patey, *J. Chem. Phys.* **111**, 9000 (1999).
- [50] A. Z. Panagiotopoulos and M. E. Fisher, *Phys. Rev. Lett.* **88**, 045701 (2002).
- [51] C. D. Daub, G. N. Patey, and P. J. Camp, *J. Chem. Phys.* **119**, 7952 (2003).
- [52] A. Kudlay, A. V. Ermoshkin, and M. Olvera de la Cruz, *Phys. Rev. E* **70**, 021504 (2004).
- [53] E. Luijten, M. E. Fisher, and A. Z. Panagiotopoulos, *Phys. Rev. Lett.* **88**, 185701 (2002).
- [54] J. Jiang, L. Blum, O. Bernard, J. M. Prausnitz, and S. I. Sandler, *J. Chem. Phys.* **116**, 7977 (2002).